Associating Borate and Silicate Chemistry by Extreme Conditions: High-Pressure Synthesis, Crystal Structure, and Properties of the New Borates $RE_3B_5O_{12}$ (RE = Er−Lu)

Holger Emme,[†] Martin Valldor,[‡] Rainer Pöttgen,[‡] and Hubert Huppertz*,[†]

Department Chemie und Biochemie, Ludwig-Maximilians-Universität München, Butenandtstrasse 5-13, D-81377 München, Germany, and Institut für Anorganische und Analytische Chemie, Westfälische Wilhelms-Universität Münster, Corrensstrasse 36, D-48149 Münster, Germany

Received December 23, 2004. Revised Manuscript Received March 15, 2005

The rare-earth borates $RE_3B_5O_{12}$ (RE = Er−Lu) were prepared by use of high-pressure and high-temperature conditions in a Walker-type multianvil apparatus at 10 GPa and 1100 °C. All compounds crystallize in a novel structure type and possess a new composition, unknown in borate chemistry until now. Interestingly, the crystal structure is homeotype to the beryllo-silicate mineral semenovite ($(Fe^{2+}$, Mn, Zn, Ti)RE_2Na_{0-2}(Ca, Na)$_8$(Si, Be)$_{20}$(O, OH, F)$_{48}$), representing an outstanding example for the realization of complex silicate structures in the field of borates by high pressure. Next to a marked pseudosymmetry, the compounds represent new examples of the rare crystallographic space group *Pmna* with only 22 exponents known so far. Fortunately, it was possible to establish single-crystal data for all compounds. The results of temperature-resolved in situ powder-diffraction measurements, quantitative analysis (ICP, EDX), DTA-TG, vibrational spectroscopy, and magnetic investigations of the new compounds are also presented.

Introduction

Boron occurs in a wide variety of igneous, sedimentary, and metamorphic mineral environments, distributed in the upper crust of the Earth. Due to the high ionization potential of boron, the bonding character is highly covalent, somewhat similar to silicon. This behavior can be attributed to the boron/silicon diagonal relationship, showing several analogies such as the condensation of $B(OH)_3$ and $Si(OH)_4$ to high-molecular acids, the formation of glasses from B_2O_3 and SiO_2, and the possibility of solving metal oxides in B_2O_3 and SiO_2 generating borates and silicates, respectively.[1]

Due to its small size, boron may reside in borates either in trigonal or in tetrahedral coordination with oxygen. Until now, it is still not clear which type of coordination is preferred under ambient conditions, where both coordinations have equal rights. Bearing in mind the pressure-coordination rule,[2] the coordination number generally increases with rising pressure. Therefore, we expect and observe that tetrahedrally coordinated boron predominates at high pressures. Due to the similar character of boron and aluminum, B^{3+} is also able to substitute aluminum in AlO_4-tetrahedra, as can be seen in the following. Due to the pressure-homologue rule,[2] high-pressure favors this substitution. For example, there are several natural and synthetic boron analogues of phases with tetrahedrally coordinated aluminum atoms; e.g., reedmergnerite $Na[BSi_3O_8]$[3,4] is the boron analogue of the feldspar albite $Na[AlSi_3O_8]$, or the paracelsian structure of danburite $Ca(B_2Si_2O_8)$,[5−8] by substituting aluminum at the tetrahedral site by boron.[9] Experiments showed that reedmergnerite is thermodynamically stable up to high pressures, about 2 GPa above those limiting the stability of albite. Investigations into the high-pressure stability of danburite demonstrated that this mineral, previously synthesized with low yields at low pressure, showed strong growth when the low-pressure product was rerun at high pressure up to 6 GPa.[10] This suggests that boron-bearing frameworks are stable phases at high pressures in agreement with the pressure-homologue rule.[2]

The diagonal-relationship B ↔ Si enables the partial substitution of silicon for boron, leading to the substance class of borosilicates, which are widespread accessory minerals, often represented by the most abundant mineral group tourmaline. Owing to its large spreading, this group is also called the "default" metamorphic borosilicate. Tourmaline is an acentric rhombohedral borosilicate, characterized by six-membered tetrahedral rings, primarily occupied by silicon.[11] Sometimes, this tetrahedral position is substituted

* To whom correspondence should be addressed. E-mail: huh@cup.uni-muenchen.de.
† Universität München.
‡ Universität Münster.

(1) Holleman, A. F.; Wiberg, E.; Wiberg, N. *Lehrbuch der Anorganischen Chemie*; Walter de Gruyter: 101st Ed., Berlin, New York, 1995.
(2) Neuhaus A. *Chimia* **1964**, *18*, 93−103.
(3) Appleman, D. E.; Clark, J. R. *Am. Mineral.* **1965**, *50*, 1827−1850.
(4) Fleet, M. E. *Am. Mineral.* **1992**, *77*, 76−84.
(5) Bakakin, V. V.; Kravchenko, V. B.; Belov, N. V. *Dokl. Akad. Nauk SSSR* **1959**, *129*, 420−423.
(6) Johansson, G. *Acta Crystallogr.* **1959**, *12*, 522−525.
(7) Phillips, M. W.; Gibbs, G. V.; Ribbe, P. H. *Am. Mineral.* **1974**, *59*, 79−85.
(8) Berger, T.; Range, K.-J. *Z. Naturforsch., B: Chem. Sci.* **1996**, *51*, 172−174.
(9) Schreyer, W.; Werding, G. *Lithos* **1997**, *41*, 251−266.
(10) Werding, G.; Schreyer, W. Reviews in Mineralogy. In *Boron: Mineralogy, Petrology, and Geochemistry*; Mineralogical Society of America: Washington, DC, 1996; Chapter 3, Vol. 33.

10.1021/cm047741+ CCC: $30.25
Published on Web 04/22/2005

for aluminum up to a level of 0.5 atoms per formula unit. There have been reports that boron may partially occupy this site in natural minerals,[12−14] but at first, spectroscopic and single-crystal structure studies have not provided compelling evidence for tetrahedrally coordinated boron in tourmaline.[15,16] In contrast, boron is positioned in slightly distorted triangular BO_3-groups, alternating over the tetrahedra at the height of the apical oxygen atoms. But in recent years, more detailed studies established the surprising fact that synthetic tourmaline phases invariably contained a large excess of boron, located in the tetrahedral ring site replacing silicon.[17,18]

Christ[19] was one of the first authors, considering the incorporation of variable amounts of boron in silicate minerals by replacing a SiO_4-tetrahedron with one unshared oxygen for $BO_3(OH)$. Later investigations exhibited that the incorporation of boron in silicates in the tetrahedral position is hardly so simple.[20]

Nevertheless, it was possible to substitute silicon for boron in mineral phases such as kornerupine,[21] of which the persistence to high pressures is solely due to the incorporation of boron into its crystal structure. Apparently, it is the boron replacing silicon in the tetrahedral site that stabilizes the kornerupine structure as a whole.[22] Thus, these minerals may represent effective sinks for boron under these extreme conditions.[23] The question of boron introduction into forsterite $Mg_2[SiO_4]$, for which Sykes et al.[24] proposed the substitution B+(F,OH) for Si+O, and the experiments of Grew et al.,[25] who found that in natural olivine (Mg, Fe)-$[SiO_4]$ up to 5% of silicon can be replaced by boron at an estimated pressure of 4 to 5 GPa, have important implications for the geochemistry of the Earth's mantle.

Unfortunately, we know very little about the incorporation of boron into micas and other phyllosilicates, about boron fractionating between such solids and the coexisting fluids, and the stability ranges of these minerals. A multitude of boron-bearing framework silicates were synthesized hunting after microporous materials for technical use. Remarkably, the boron atoms have largely migrated out of the center of the tetrahedra to form BO_3 groups.

Against this background, one wonders about the influence of pressure on boron introduction into other silicates or the stabilization of borates with structures similar to existing silicates. Generally, there are synthetic boron micas such as boron muscovite[26,27] $KAl_2[BSi_3O_{10}](OH)_2$, but an entire exchange of aluminum and silicon for boron is realized in none of them. Here we report the high-pressure/high-temperature synthesis and characterization of four new borates with the composition $RE_3B_5O_{12}$ (RE = Er−Lu), exhibiting a structure type homeotype to the beryllo-silicate semenovite $((Fe^{2+}, Mn, Zn, Ti)RE_2Na_{0-2}(Ca, Na)_8(Si, Be)_{20}(O, OH, F)_{48})$.[28,29] Apparently, extreme conditions of 10 GPa and 1100 °C enable the formation of layers, built up solely from tetrahedra analogous to semenovite, in which, for the first time, silicon/beryllium is completely substituted for boron. Additionally, $RE_3B_5O_{12}$ represents a new composition in the system RE_2O_3/B_2O_3, unknown so far (for an overview see ref 36). Earlier investigations in our group showed that the utilization of high-pressure/high-temperature conditions in the synthesis of borates can lead to new metastable but tangible borates with new compositions and special structural motifs. New high-pressure polymorphs such as χ-$REBO_3$ (RE = Dy−Er), which contain layers built up from noncyclic $[B_3O_9]^{9-}$-anions,[30] or new meta-borates such as β-$RE(BO_2)_3$ (RE = Dy−Lu),[31,32] and γ-$RE(BO_2)_3$ (RE = La−Nd),[33,34] allowed us to look at new preparative possibilities under these extreme conditions. The synthesis of compositions such as $RE_4B_6O_{15}$ (RE = Dy, Ho)[35−37] and α-$RE_2B_4O_9$ (RE = Eu−Dy),[38−40] where the new structural motif of edge-sharing BO_4-tetrahedra was observed for the first time, favored systematic investigations in this field.

During our investigations of the stability fields of the metaborates $RE(BO_2)_3$, we synthesized the isotypic higher homologues of the orthorhombic phases β-$RE(BO_2)_3$ with RE = Dy−Lu by high pressure.[31] In this area, only the compounds β-$RE(BO_2)_3$ (RE = Dy−Er) were obtained as single-phase products, whereas the orthorhombic species with RE = Tm−Lu crystallized as byproducts next to new high-pressure phases, which were identified as $RE_3B_5O_{12}$ (RE = Tm−Lu). In this paper, we report the optimized syntheses, crystal structures, and properties of the new borates $RE_3B_5O_{12}$

(11) Henry, D. J.; Dutrow, B. L. Reviews in Mineralogy. In *Boron: Mineralogy, Petrology, and Geochemistry*; Mineralogical Society of America: Washington, DC, 1996; Chapter 10, Vol. 33.
(12) Barton, P., Jr. *Acta Crystallogr., Sect. B: Struct. Sci.* **1969**, *25*, 1524−1533.
(13) Palmer, M. R.; London, D.; Morgan, G. B.; Babb, H. A. *Chem. Geol. Isotope Geosci. Sect.* **1992**, *101*, 123−129.
(14) Dyar, M. D.; Francis, C. A.; Wise, M. A.; Guidotti, C. V.; McGuire, A. V.; Robertson, J. D. *Trans. Am. Geophys. Union* **1994**, *75*, 187.
(15) Tsang, T.; Ghose, S. *Am. Mineral.* **1973**, *58*, 224−229.
(16) Hawthorne, F. C. *Can. Mineral.* **1996**, *34*, 123−132.
(17) Marler, B.; Borowski, M.; Wodara, U.; Schreyer, W. *Eur. J. Mineral.* **2002**, *14*, 763−771.
(18) Schreyer, W.; Hughes, J. M.; Bernhardt, H.-J.; Kalt, A.; Prowatke, S.; Ertl, A. *Eur. J. Mineral.* **2002**, *14*, 935−942.
(19) Christ, C. L. *Norsk. Geol. Tidsskrift* **1965**, *45*, 423−428.
(20) Grew, E. S. Reviews in Mineralogy. In *Boron: Mineralogy, Petrology, and Geochemistry*; Mineralogical Society of America: Washington, DC, 1996; Chapter 9, Vol. 33.
(21) Moore, P. B.; Bennett, J. M. *Science* **1968**, *159*, 524−526.
(22) Klaska, R.; Grew, E. S. *Am. Mineral.* **1991**, *76*, 1824−1835.
(23) Schreyer, W.; Stöckhert, B. *Lithos* **1997**, *41*, 1−4.
(24) Sykes, D.; Rossman, G. R.; Veblen, D. R.; Grew, E. S. *Am. Mineral.* **1994**, *79*, 904−908.
(25) Grew, E. S.; Pertsev, N. N.; Boronikhin, V. A.; Borisovskiy, S. Y.; Yates, M. G.; Marquez, N. *Am. Mineral.* **1991**, *76*, 1061−1080.
(26) Foord, E. E.; Martin, R. F.; Fitzpatrick, J. J.; Taggart, J. E.; Crock, J. G. *Am. Mineral.* **1991**, *76*, 1998−2002.
(27) Stubican, V.; Roy, R. *Am. Mineral.* **1962**, *47*, 1166−1173.
(28) Petersen, O. V.; Rönsbo, J. G. *Lithos* **1972**, *5*, 163−173.
(29) Mazzi, F.; Ungaretti, L.; Dal Negro, A.; Petersen, O. V.; Rönsbo, J. G. *Am. Mineral.* **1979**, *64*, 202−210.
(30) Huppertz, H.; von der Eltz, B.; Hoffmann, R.-D.; Piotrowski, H. *J. Solid State Chem.* **2002**, *166*, 203−212.
(31) Emme, H.; Nikelski, T.; Schleid, Th.; Pöttgen, R.; Möller, M. H.; Huppertz, H. *Z. Naturforsch., B: Chem. Sci.* **2004**, *59*, 202−215.
(32) Nikelski, T.; Schleid, Th. *Z. Anorg. Allg. Chem.* **2003**, *629*, 1017−1022.
(33) Emme, H.; Despotopoulou, C.; Huppertz, H. *Z. Anorg. Allg. Chem.* **2004**, *630*, 1717.
(34) Emme, H.; Despotopoulou, C.; Huppertz, H. *Z. Anorg. Allg. Chem.* **2004**, *630*, 2450−2457.
(35) Huppertz, H.; von der Eltz, B. *J. Am. Chem. Soc.* **2002**, *124*, 9376−9377.
(36) Huppertz, H. *Z. Naturforsch., B: Chem. Sci.* **2003**, *58*, 278−290.
(37) Huppertz, H.; Emme, H. *J. Phys.: Condens. Matter* **2004**, *16*, S1283−S1290.
(38) Emme, H.; Huppertz, H. *Z. Anorg. Allg. Chem.* **2002**, *628*, 2165.
(39) Emme, H.; Huppertz, H. *Chem. Eur. J.* **2003**, *9*, 3623−3633.
(40) Emme, H.; Huppertz, H. *Acta Crystallogr., Sect. C: Struct. Commun.* **2005**, 61, i29−i31.

(RE = Er−Lu) with a special view of the analogies to the beryllo-silicate mineral semenovite.

Experimental Section

Synthesis. According to eq 1, the starting materials for the synthesis of $RE_3B_5O_{12}$ (RE = Er−Lu) were stoichiometric mixtures of B_2O_3 [Strem Chemicals, Newburyport, U.S.A., 99.9%] with the rare-earth oxides RE_2O_3 (RE = Er−Lu) [99.9%].

$$3\ RE_2O_3 + 5\ B_2O_3 \xrightarrow[1100\ °C]{10\ GPa} 2\ RE_3B_5O_{12}\ (RE = Er{-}Lu) \quad (1)$$

The starting materials were compressed and heated in a multianvil assembly (18/11) with a modified Walker module and a 1000 t press (Voggenreiter, Mainleus, Germany). Precast MgO octahedra (Ceramic Substrates & Components, Isle of Wight, UK) with an edge length of 18 mm were used as a pressure medium. Eight tungsten carbide cubes (TSM 10, Ceratizit, Austria) with a truncation of 11 mm, separated by pyrophyllite gaskets, compressed the octahedra (18/11 assembly in conventional terminology). The mixtures (each ≈100 mg) were filled into cylindrical boron nitride crucibles that were sealed by a boron nitride plate. The sample cylinders were placed at the center of cylindrical resistance heaters (graphite) that had a variable stepped wall thickness to minimize the thermal gradient along the sample. MgO rods filled the space on the top and bottom of the samples. Thermal insulation was provided by a cylindrical zirconia sleeve that surrounded the furnace. The assemblies were positioned inside the octahedra and placed in contact with a molybdenum ring at the top and a molybdenum plate at the bottom. The experimental temperature was monitored by means of $Pt/Pt_{87}Rh_{13}$ thermocouples that were inserted axially into the octahedral assemblies, with the hot junctions being in contact with the boron nitride cylinders. Further details of the construction of the assemblies can be found in refs 41−45. For the synthesis of $RE_3B_5O_{12}$ (RE = Er−Lu), the assemblies were compressed within 3 h to 10 GPa and heated to 1000 °C in the following 10 min. After this temperature was held for 10 min, the samples were cooled to room temperature within another 10 min. After decompression, the recovered experimental octahedra were broken apart, and the samples were carefully separated from the surrounding hexagonal boron nitride. The compounds $RE_3B_5O_{12}$ (RE = Er−Lu) were obtained as crystalline products (yield: ca. 75 mg per run). The air- and humidity-resistant substances crystallize as thin, pink (Er), and colorless (Tm−Lu) plates.

Physical Measurements. X-ray Diffraction. Small single crystals of $RE_3B_5O_{12}$ (RE = Er−Lu) were isolated by mechanical fragmentation and examined by Buerger precession photographs. Single-crystal intensity data of $RE_3B_5O_{12}$ (RE = Er, Lu) were measured with an Enraf-Nonius Kappa CCD, equipped with a rotating anode [Mo Kα radiation (71.073 pm)] at room temperature. The crystals of the thulium and ytterbium compound were measured with a STOE-IPDS I or II area detector diffractometer [Mo Kα radiation (71.073 pm)]. A look on the integral reflection conditions with the Program XPREP [46] favored a *B*-centered cell, but a more precise analysis exhibited weak reflections, violating $h + l = 2n$. In the primitive setting the systematic extinctions $h0l$ with $h + l \neq 2n$ and $hk0$ with $h \neq 2n$ led to the space groups *P*2*na* (No. 30; standard setting: *Pnc*2) and *Pmna* (No. 53). The centrosymmetric group was found to be correct during the refinement. This was confirmed with the ADDSYM routine of the program PLATON.[47]

Structure solution and parameter refinement (full-matrix least-squares against F^2) were successfully performed on all four compounds, using the SHELX-97 software suite.[48] Details of the data collections and structure refinements are listed in Table 1. Additionally, the positional parameters (Table 2), anisotropic displacement parameters (Table 3), interatomic distances (Tables 4 and 5), and interatomic angles (Table 6) are given in detail for $Lu_3B_5O_{12}$.

Powder diffraction patterns of $RE_3B_5O_{12}$ (RE = Er−Lu) were obtained from 0.2 mm Mark capillaries using a STOE STADI P powder diffractometer with monochromatized Mo Kα radiation. The diffraction patterns were indexed with the program ITO[49] on the basis of an orthorhombic unit cell. The lattice parameters (Tables 1 and 7) were calculated from least-squares fits of the powder data. The correct indexing of the patterns of $RE_3B_5O_{12}$ (RE = Er−Lu) was confirmed by intensity calculations, taking the atomic positions from the structure refinement.[50] The lattice parameters for all compounds, determined from the powder data and single-crystal data, tally well.

Temperature-dependent X-ray powder diffraction experiments were performed on a STOE Stadi P powder diffractometer (Mo Kα) with a computer-controlled STOE furnace: The sample was enclosed in a quartz capillary and heated from room temperature to 1100 °C in 100 °C steps. At each temperature a diffraction pattern was recorded over the angular range $8° \leq 2\theta \leq 17°$.

Quantitative Analysis. The composition of the new compound $RE_3B_5O_{12}$ (RE = Yb), with respect to the elements ytterbium and boron, was verified with ICP (inductively coupled plasma) on a VARIAN-VISTA-Spectrometer and additionally by EDX analysis on a JEOL JSM-6500F.

Thermoanalytical Investigations. The DTA-TG curves of $RE_3B_5O_{12}$ (RE = Yb) were recorded between room temperature and 1200 °C with a heating rate of 10 °C min^{-1}, using a Setaram TGA 92-2400 combined DTA-TG-thermobalance.

Vibrational Spectroscopy. A FTIR spectrum of $RE_3B_5O_{12}$ (RE = Yb) was obtained at room temperature by using a Bruker IFS 66v/S spectrometer with DTGS detector. The sample was thoroughly mixed with dried KBr (5 mg of the sample, 500 mg of KBr). The preparation procedure was performed in a glovebox under a dried argon atmosphere. The spectrum was collected in a range from 400 to 4000 cm^{-1} with a resolution of 2 cm^{-1}. During the measurement, the sample chamber was evacuated.

Magnetic Measurements. The magnetic susceptibility of a polycrystalline, powdered sample of $Yb_3B_5O_{12}$ was measured in the temperature range 3−300 K in a 1 T dc field using a Quantum Design Physical Property Measurement System. A quantity of 43.95 mg was enclosed in a small gelatine capsule and fixed at the sample holder rod. The sample was then cooled in a zero magnetic field and slowly heated to room temperature in the applied external field.

Results and Dicussion

Crystal Structure. Figure 1 gives a view of the crystal structure of $RE_3B_5O_{12}$ (RE = Er−Lu) along [001]. The structure is based on layers of condensed BO_4-tetrahedra

(41) Huppertz, H. *Z. Naturforsch., B: Chem. Sci.* **2001**, *56*, 697−703.
(42) Walker, D.; Carpenter, M. A.; Hitch, C. M. *Am. Mineral.* **1990**, *75*, 5, 1020−1028.
(43) Walker, D. *Am. Mineral.* **1991**, *76*, 1092−1100.
(44) Rubie, D. C. *Phase Transitions* **1999**, *68*, 431−451.
(45) Huppertz, H. *Z. Kristallogr.* **2004**, *219*, 330−338.
(46) *XPREP*, Version 5.04. Siemens Analytical X-ray Instruments Inc.: Madison, WI, 1990−1996.
(47) Spek, A. L. *PLATON−A Multipurpose Crystallographic Tool*; Utrecht University: Utrecht, The Netherlands, 2002.
(48) Sheldrick, G. M. *SHELXS97 and SHELXL97−Program suite for the solution and refinement of crystal structures*; University of Göttingen: Göttingen, Germany, 1997.
(49) Visser, J. W. *J. Appl. Crystallogr.* **1969**, *2*, 89−95.
(50) *WinX^{POW} Software*; STOE & CIE GmbH: Darmstadt, Germany, 1998.

Table 1. Crystal Data and Structure Refinement for $RE_3B_5O_{12}$ (RE = Er−Lu)

empirical formula	$Er_3B_5O_{12}$	$Tm_3B_5O_{12}$	$Yb_3B_5O_{12}$	$Lu_3B_5O_{12}$
molar mass/g·mol^{-1}	747.83	752.84	765.17	770.96
crystal system	orthorhombic			
space group	*Pmna* (No. 53)			
powder diffractometer	Stoe Stadi P			
radiation	Mo Kα (λ = 71.073 pm)			
powder diffraction data				
a/pm	1286.1(5)	1280.5(4)	1277.8(2)	1274.7(5)
b/pm	462.2(2)	460.2(2)	458.96(4)	457.1(2)
c/pm	1253.1(4)	1248.1(4)	1245.1(2)	1242.4(5)
volume/nm^3	0.7449(6)	0.7355(5)	0.7302(2)	0.7240(7)
single-crystal diffractometer	Nonius Kappa CCD	STOE IPDS I	STOE IPDS II	Nonius Kappa CCD
radiation	Mo Kα (λ = 71.073 pm)			
single-crystal data				
a/pm	1284.6(2)	1282.0(3)	1277.4(3)	1276.5(2)
b/pm	461.9(2)	460.19(9)	458.64(9)	457.5(2)
c/pm	1251.3(2)	1247.7(3)	1245.1(3)	1244.2(2)
volume/nm^3	0.7424(2)	0.7361(3)	0.7295(3)	0.7266(2)
formula units per cell	$Z = 4$			
temperature/K	293(2)	293(2)	293(2)	200(2)
calculated density/g·cm^{-3}	6.691	6.793	6.967	7.048
crystal size/mm^3	0.02 × 0.02 × 0.02	0.10 ×0.05 × 0.04	0.10 × 0.02 × 0.05	0.11 × 0.04 × 0.02
detector distance/mm	30.0	40.0	60.0	50.0
exposure time per plate/min		3.0	50.0	
exposure time per deg/s	50.0			17.0
absorption coefficient/mm^{-1}	33.69	35.93	38.23	40.53
F(000)	1300	1312	1324	1336
θ range/°	3.2−32.1	4.6−32.9	3.2−34.9	3.2−37.5
range in *hkl*	±19, ±6, ±18	±19, ±6, ±19	−19/+20, ±7,−16/+18	±21, ±7, ±21
scan type	φ/ω	φ/ω	ω	φ/ω
total no. reflections	14145	8905	9635	14453
independent reflections	1301 (R_{int} = 0.0589)	1412 (R_{int} = 0.0521)	1551 (R_{int} = 0.0770)	1928 (R_{int} = 0.0569)
reflections with $I > 2\sigma(I)$	840 (R_σ = 0.0382)	751 (R_σ = 0.0344)	1061 (R_σ = 0.0371)	1141 (R_σ = 0.0365)
data/parameters	1301/90	1412/95	1551/90	1928/101
absorption correction	numerical (HABITUS)[77]			
goodness-of-fit (F^2)	1.033	0.814	1.182	0.957
final *R* indices [$I > 2\sigma(I)$]	R1 = 0.0252	R1 = 0.0376	R1 = 0.0445	R1 = 0.0290
	wR2 = 0.0571	wR2 = 0.0922	wR2 = 0.0982	wR2 = 0.0776
R indices (all data)	R1 = 0.0464	R1 = 0.0642	R1 = 0.0670	R1 = 0.0566
	wR2 = 0.0651	wR2 = 0.1001	wR2 = 0.1084	wR2 = 0.0850
extinction coefficient	0.00172(8)	0.0043(2)	0.0089(4)	0.00070(9)
larg. diff. peak and hole/e·Å^{-3}	2.17/−2.89	3.17/−5.78	4.62/−2.72	6.43/−5.02

Table 2. Atomic Coordinates and Isotropic Equivalent Displacement Parameters U_{eq}/Å^2 for $Lu_3B_5O_{12}$ (Space Group: *Pmna*)[a]

atom	Wyckoff position	*x*	*y*	*z*	U_{eq}
Lu1	4*e*	0.13248(2)	0	1/2	0.00495(8)
Lu2	8*i*	0.36456(1)	0.99877(6)	0.69365(1)	0.00552(7)
B1	4*f*	0.3381(5)	1/2	1/2	0.006(2)
B2	8*i*	0.2980(5)	0.472(2)	0.8497(4)	0.008(2)
B3	4*h*	0	0.461(2)	0.3516(6)	0.005(2)
B4	4*h*	0	0.541(2)	0.8744(7)	0.008(2)
O1	4*h*	0	0.245(2)	0.4303(4)	0.0087(9)
O2	4*h*	0	0.238(2)	0.8617(4)	0.009(2)
O3	8*i*	0.2963(3)	0.7799(8)	0.8485(2)	0.0079(7)
O4	8*i*	0.4049(3)	0.3366(9)	0.8546(3)	0.0090(7)
O5	8*i*	0.4042(2)	0.3326(8)	0.4266(3)	0.0079(6)
O6	4*g*	1/4	0.339(2)	3/4	0.0078(9)
O7	4*h*	1/2	0.695(2)	0.7388(4)	0.0077(9)
O8	8*i*	0.2664(2)	0.3093(7)	0.5644(3)	0.0079(6)

[a] U_{eq} is defined as one-third of the trace of the orthogonalized U_{ij} tensor.

Table 3. Anisotropic Displacement Parameters/Å^2 for $Lu_3B_5O_{12}$ (Space Group: *Pmna*)

atom	U_{11}	U_{22}	U_{33}	U_{12}	U_{13}	U_{23}
Lu1	0.0050(2)	0.0050(2)	0.0049(2)	0	0	0.0002(2)
Lu2	0.0051(2)	0.0054(2)	0.0061(2)	0.00002(9)	0.00024(6)	−0.0002(2)
B1	0.005(2)	0.009(3)	0.005(2)	0	0	0.000(4)
B2	0.004(2)	0.013(3)	0.006(2)	0.003(2)	−0.001(2)	−0.004(2)
B3	0.004(3)	0.005(4)	0.006(3)	0	0	−0.003(2)
B4	0.010(3)	0.006(5)	0.006(3)	0	0	0.003(2)
O1	0.009(2)	0.012(3)	0.005(2)	0	0	0.000(2)
O2	0.011(2)	0.006(2)	0.012(2)	0	0	0.004(2)
O3	0.009(2)	0.009(2)	0.007(2)	0.000(2)	−0.000(2)	0.000(2)
O4	0.008(2)	0.007(2)	0.012(2)	0.001(2)	0.001(2)	0.002(2)
O5	0.005(2)	0.008(2)	0.011(2)	−0.002(2)	0.002(2)	0.001(2)
O6	0.009(2)	0.006(2)	0.008(2)	0	0.002(2)	0
O7	0.008(2)	0.008(2)	0.007(2)	0	0	0.000(2)
O8	0.008(2)	0.007(2)	0.008(2)	0.002(2)	0.001(2)	−0.002(2)

Table 4. Interatomic B−O Distances/pm Calculated with the Single-Crystal Lattice Parameters in $Lu_3B_5O_{12}$ (Standard Deviations in Parentheses)

B1−O5a	146.0(5)	B2−O3	141.1(7)	B3−O1	139.2(9)	B4−O2	139.3(9)
B1−O5b	146.0(5)	B2−O4a	149.9(7)	B3−O4a	152.7(6)	B4−O5a	150.1(6)
B1−O8a	149.7(5)	B2−O6	151.2(6)	B3−O4b	152.7(6)	B4−O5c	150.1(6)
B1−O8b	149.7(5)	B2−O8a	153.9(7)	B3−O7a	157.5(8)	B4−O7b	157.5(9)
	∅ 147.9		∅ 149.0		∅ 150.5		∅ 149.3

∅ over all distances 149.2

separated by rare-earth cations. Due to the pressure coordination rule, we exclusively observe the presence of BO_4-tetrahedra as in the crystal structures of $RE_4B_6O_{15}$ (RE = Dy, Ho),[35−37] α-$RE_2B_4O_9$ (RE = Eu−Dy),[38,39] β-$RE(BO_2)_3$ (RE = Tb−Lu),[31,32] and γ-$RE(BO_2)_3$ (RE = La−Nd).[33,34] Three kinds of BO_4-tetrahedra rings are formed within the layers: four-membered, five-membered, and eight-membered rings (Figure 2). The four-membered rings lie in the *ac*-plane in the center and on the edges of the unit cell along *b* at a height of 1/2. Only the tetrahedron around B(1) (Q^4, dark polyhedra) shares all vertexes with other tetrahedra, whereas the remaining ones (B(2)−B(4)) (Q^3, light shaded polyhedra) have one unshared oxygen atom. Inside the four-membered ring Q^4 (B1) and Q^3 (B2) tetrahedra occur on alternate positions. Two adjacent tetrahedra of the four-membered ring build up a five-membered ring at a time with three additional BO_4-tetrahedra (Q^3). Furthermore, two Q^4 and six Q^3 tetrahedra form eight-membered rings, connecting the four-membered rings along the *a*-axis, and separating pairs of five-membered rings along the *c*-axis.

Table 5. Interatomic Lu−O Distances/pm Calculated with the Single-Crystal Lattice Parameters in $Lu_3B_5O_{12}$ (Standard Deviations in Parentheses)

Lu1−O1a	220.6(3)	Lu2−O2	216.0(3)
Lu1−O1b	220.6(3)	Lu2−O5	218.9(4)
Lu1−O3a	232.2(3)	Lu2−O6	224.6(3)
Lu1−O3b	232.2(3)	Lu2−O7	228.7(3)
Lu1−O8a	235.9(3)	Lu2−O3a	234.0(3)
Lu1−O8b	235.9(3)	Lu2−O3b	234.4(4)
Lu1−O4a	242.3(4)	Lu2−O8	248.5(3)
Lu1−O4b	242.3(4)	Lu2−O4	258.2(4)
	∅ 232.8		∅ 232.9

∅ over all distances 232.8

Table 6. Interatomic Angles/° Calculated with the Single-Crystal Lattice Parameters in $Lu_3B_5O_{12}$ (Standard Deviations in Parentheses)

O5a−B1−O5b	109.4(5)	O3−B2−O4a	115.2(5)	O1−B3−O4a	114.4(4)
O5a−B1−O8a	108.9(2)	O3−B2−O6	112.8(4)	O1−B3−O4b	114.4(4)
O5a−B1−O8b	112.5(2)	O4a−B2−O6	103.7(4)	O4a−B3−O4b	105.3(6)
O5b−B1−O8b	112.5(2)	O3−B2−O8a	118.8(4)	O1−B3−O7a	107.8(5)
O5b−B1−O8a	108.9(2)	O4a−B2−O8a	105.1(4)	O4a−B3−O7a	107.3(4)
O8a−B1−O8b	104.6(5)	O6−B2−O8a	99.1(4)	O4b−B3−O7a	107.3(4)
	∅ 109.5		∅ 109.1		∅ 109.4
O2−B4−O5a	115.6(4)				
O2−B4−O5c	115.6(4)				
O5a−B4−O5c	109.1(6)		∅ over all angles 109.3		
O2−B4−O7b	110.2(6)				
O5a−B4−O7b	102.4(4)				
O5c−B4−O7b	102.4(4)				
	∅ 109.2				

Table 7. Comparison of the Lattice Parameters/pm and Volumes/nm³ of $RE_3B_5O_{12}$ (RE = Er−Lu)

compound	*a*	*b*	*c*	*V*
$Er_3B_5O_{12}$	1286.1(5)	462.2(2)	1253.1(4)	0.7449(6)
$Tm_3B_5O_{12}$	1280.5(4)	460.2(2)	1248.1(4)	0.7355(5)
$Yb_3B_5O_{12}$	1277.8(2)	458.96(4)	1245.1(2)	0.7302(2)
$Lu_3B_5O_{12}$	1274.7(5)	457.1(2)	1242.4(5)	0.7240(7)

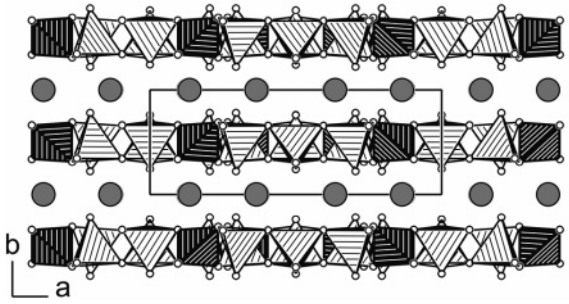

Figure 1. Crystal structure of $RE_3B_5O_{12}$ (RE = Er−Lu); view along [001]. Light shaded polyhedra represent Q^3 bonded BO_4-tetrahedra; dark polyhedra show Q^4-tetrahedra.

The coordination polyhedra around the RE^{3+} ions are both distorted square antiprisms (Figure 3) with RE−O distances of 218−261 pm for RE = Er, 217−261 pm for RE = Tm, 216−260 pm for RE = Yb, and 216−258 pm for RE = Lu (Table 5). The decreasing interatomic distances on going from RE = Er to Lu reflect the lanthanide contraction. Figure 2 shows that the cations are positioned between the five- and eight-membered rings.

The B−O bond lengths in $RE_3B_5O_{12}$ (RE = Er−Lu) vary between 138 and 159 pm ($Er_3B_5O_{12}$), 139 and 157 pm ($Tm_3B_5O_{12}$), 140 and 158 pm ($Yb_3B_5O_{12}$), and 139 and 158 pm ($Lu_3B_5O_{12}$) (Table 4). The average B−O bond length of each compound with the values 149.4 pm (RE = Er, Tm), 148.9 pm (RE = Yb), and 149.2 pm (RE = Lu) (Table 4) are slightly larger in comparison to the known average value

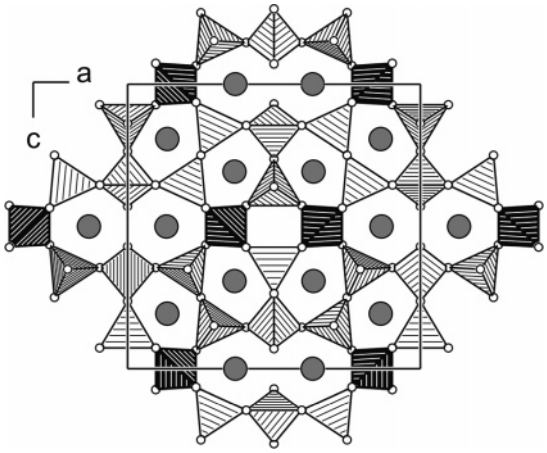

Figure 2. Crystal structure of $RE_3B_5O_{12}$ (RE = Er−Lu); view along [010]. Light shaded polyhedra represent Q^3 bonded BO_4-tetrahedra; dark polyhedra show Q^4-tetrahedra.

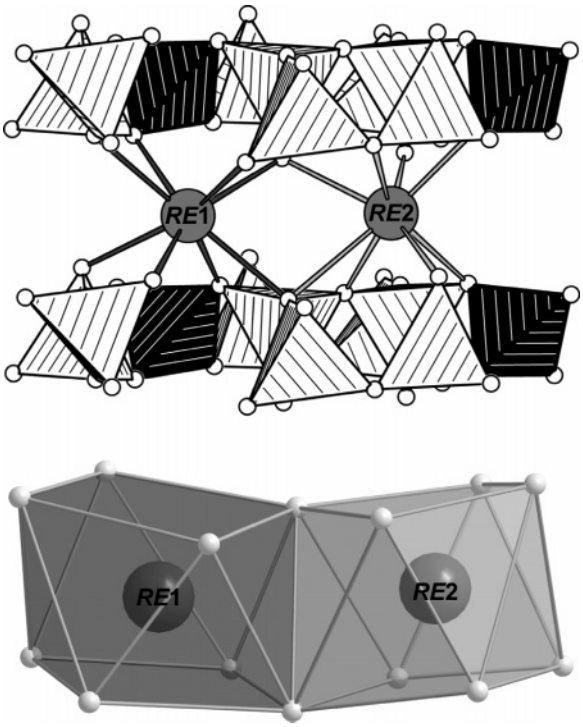

Figure 3. Coordination spheres of RE^{3+} (gray spheres) in the crystal structure of $RE_3B_5O_{12}$ (RE = Er−Lu) (top) and the corresponding coordination polyhedra (bottom).

of 147.0 pm for borates.[51,52] The O−B−O angles in the BO_4-tetrahedra vary between 99.8 and 117.3° for $Er_3B_5O_{12}$, 98.2 and 118.2° for $Tm_3B_5O_{12}$, 99.6 and 117.3° for $Yb_3B_5O_{12}$, and 99.1 and 118.8° for $Lu_3B_5O_{12}$ (Table 6). These strong deviations from the ideal tetrahedron angle are not exceptional for rare-earth borates, synthesized under extreme conditions. Examples for such strongly distorted tetrahedra in BO_4-networks can be found in the high-pressure phases α-$RE_2B_4O_9$ (RE = Eu−Tb) with O−B−O angles varying between 99.5 and 118.9° for α-$Eu_2B_4O_9$, 99.4 and 119.0° for α-$Gd_2B_4O_9$, and 99.4 and 119.4° for α-$Tb_2B_4O_9$.[37−39]

(51) Hawthorne, F. C.; Burns, P. C.; Grice, J. D. Reviews in Mineralogy. In *Boron: Mineralogy, Petrology, and Geochemistry*; Mineralogical Society of America: Washington, DC, 1996; Chapter 2, Vol. 33.
(52) Zobetz, E. *Z. Kristallogr.* **1990**, *191*, 45−57.

Table 8. Cycle-Class Sequences of $RE_3B_5O_{12}$ (RE = Er−Lu) and Semenovite (Fe^{2+}, Mn, Zn, Ti)RE_2Na_{0-2}(Ca, Na)$_8$(Si, Be)$_{20}$((O, OH, F)$_{48}$ [60−63]

ring size	3	4	5	6	7	8	9	10	11
$RE_3B_5O_{12}$	0	2	8	0	8	14	0	16	40
semenovite	0	4	15	0	15	24	0	28	63

Table 9. Charge Distribution in $RE_3B_5O_{12}$ (RE = Er−Lu) Calculated with the Bond-Length/Bond-Strength Concept (ΣV)[53,54] and the CHARDI Concept (ΣQ)[55]

	ΣV	ΣQ		ΣV	ΣQ		ΣV	ΣQ		ΣV	ΣQ
Er1	+3.23	+3.06	Tm1	+3.25	+3.05	Yb1	+3.21	+3.03	Lu1	+3.12	+3.03
Er2	+3.37	+2.93	Tm2	+3.36	+2.91	Yb2	+3.30	+2.93	Lu2	+3.23	+2.92
B1	+2.94	+3.09		+2.99	+3.12		+3.03	+3.11		+2.99	+3.08
B2	+2.95	+3.01		+2.94	+3.00		+2.94	+3.01		+2.92	+3.01
B3	+2.74	+3.10		+2.78	+3.12		+2.81	+3.07		+2.83	+3.12
B4	+2.95	+2.89		+2.90	+2.89		+2.96	+2.91		+2.93	+2.91
O1	−2.00	−2.11		−2.01	−2.07		−2.14	−2.16		−2.12	−2.14
O2	−2.24	−2.24		−2.20	−2.21		−2.28	−2.19		−2.28	−2.20
O3	−2.03	−2.01		−2.09	−2.12		−2.10	−2.03		−2.14	−2.08
O4	−1.88	−1.85		−1.87	−1.84		−1.91	−1.84		−1.90	−1.80
O5	−2.19	−2.05		−2.06	−2.05		−2.10	−2.04		−2.11	−2.05
O6	−2.40	−2.34		−2.32	−2.25		−2.43	−2.33		−2.42	−2.28
O7	−2.04	−1.84		−2.05	−1.89		−2.13	−1.89		−2.10	−1.83
O8	−1.95	−1.82		−1.94	−1.78		−1.99	−1.80		−2.01	−1.84

Table 10. MAPLE Values/kJ·mol^{-1} of $RE_3B_5O_{12}$ (RE = Er−Lu) in Comparison with the MAPLE Values/kJ·mol^{-1} of the Binary Oxides RE_2O_3 (RE = Er−Lu) and the High-Pressure Modification B_2O_3−II, and Their Deviation/%[56−58]

compound	calculated MAPLE	MAPLE from binary oxides	deviation
$Er_3B_5O_{12}$	77809	77870	0.08
$Tm_3B_5O_{12}$	77879	78121	0.30
$Yb_3B_5O_{12}$	78088	78152	0.08
$Lu_3B_5O_{12}$	78047	78229	0.23

For further clarification, we calculated bond-valence sums for $RE_3B_5O_{12}$ (RE = Er−Lu) with the bond length/bond strength and CHARDI concept (Table 9).[53−55] The formal ionic charges of the atoms, acquired by the X-ray structure analysis, are in agreement within the limits of the concepts. Additionally, we calculated MAPLE values (Madelung Part of Lattice Energy)[56−58] for $RE_3B_5O_{12}$ (RE = Er−Lu) in order to compare them with MAPLE values from the binary compounds RE_2O_3 (RE = Er−Lu) and the high-pressure modification B_2O_3−II (Table 10). Foundation therefore is the additive potential of the MAPLE values, whereby it is possible to calculate hypothetical values for $RE_3B_5O_{12}$ (RE = Er−Lu) starting from the binary oxides. Table 10 shows the results of the calculated values starting from the structural parameters given in this paper in comparison to the values based on the binary components. The deviations of the values are in the range 0.08−0.30%.

Figure 4 and Table 7 give an impression of the development of the lattice parameters in $RE_3B_5O_{12}$ (RE = Er−Lu). Due to the lanthanide contraction and the layered character

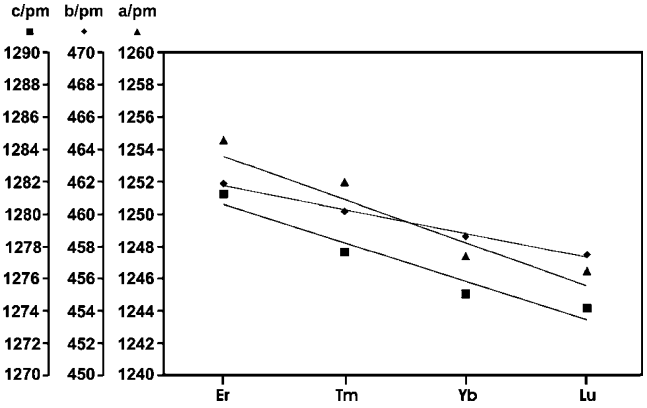

Figure 4. Plot of the lattice parameters of the rare-earth borates $RE_3B_5O_{12}$ (RE = Er−Lu) (single-crystal data).

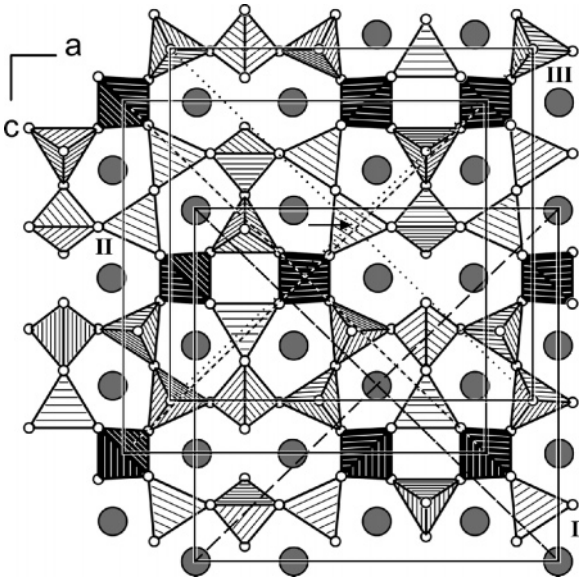

Figure 5. Visualization of the pseudosymmetry in the crystal structure of $RE_3B_5O_{12}$ (RE = Er−Lu). Frame I: *B*-centering of the RE^{3+} ions; frame II: *B*-centering of the boron cations; frame III: violation of the *B*-centering by the oxygen atoms.

of the structure along [010], the cell parameters *a*, *b*, and *c* across the series Er to Lu decrease by 0.9, 1.1, and 0.9%, respectively. As expected, there is only a small difference among the values with the largest percentage contraction between the layers (along [010]).

In the beginning of our structural investigations, we had serious problems with a *B*-face-centered pseudosymmetry inside the structure of $RE_3B_5O_{12}$ (RE = Er−Lu) (see section on X-ray Diffraction). Figure 5 exhibits clearly that the rare-earth cations (frame I) and the boron atoms inside the tetrahedra (frame II) fulfill the *B*-centering; however, as is evident from frame III, the oxygen atoms violate the *B*-face centering. On the corners of frame III, all tetrahedra point toward the observer (up), whereas the tetrahedron in the center of the frame (see arrow) has the opposite orientation (down). Semenovite shows a similar pseudosymmetry, possessing a nearly body-centered structure.

Though $RE_3B_5O_{12}$ (RE = Er−Lu) crystallizes in a new structure type for borates, there is an interesting homeotype structure known from the beryllo-silicate mineral semenovite ((Fe^{2+}, Mn, Zn, Ti)RE_2Na_{0-2}(Ca, Na)$_8$(Si, Be)$_{20}$(O, OH, F)$_{48}$) (Figure 6),[28,29] which consists of topologically identical

(53) Brown, I. D.; Altermatt, D. *Acta Crystallogr., Sect. B: Struct. Sci.* **1985**, *41*, 244−247.
(54) Brese, N. E.; O'Keeffe, M. *Acta Crystallogr., Sect. B: Struct. Sci.* **1991**, *47*, 192−197.
(55) Hoppe, R.; Voigt, S.; Glaum, H.; Kissel, J.; Müller, H. P.; Bernet, K. *J. Less-Common Met.* **1989**, *156*, 105−122.
(56) Hoppe, R. *Angew. Chem.* **1966**, *78*, 52−63; *Angew. Chem., Int. Ed.* **1966**, *5*, 96−106.
(57) Hoppe, R. *Angew. Chem.* **1970**, *82*, 7−16; *Angew. Chem., Int. Ed.* **1970**, *9*, 25−34.
(58) Hübenthal, R. *MAPLE−Program for the Calculation of MAPLE Values*, Vers. 4; University of Giessen: Giessen, Germany, 1993.

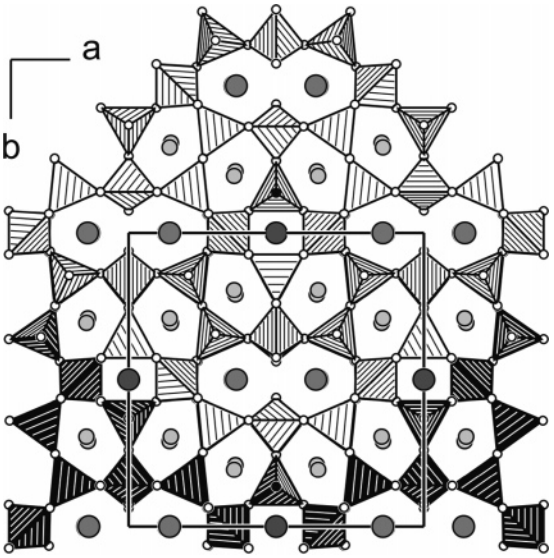

Figure 6. Crystal structure of the mineral semenovite, (Fe^{2+}, Mn, Zn, Ti)RE_2Na_{0-2} (Ca, Na)$_8$(Si, Be)$_{20}$(O, OH, F)$_{48}$, view along [001] (space group: *Pmnn*) ((Si, Be)O_4-tetrahedra, oxygen, white spheres; fluorine, black spheres; (calcium, sodium): light gray spheres; (rare-earth, sodium): medium gray spheres; (iron, manganese, zinc, titanium): dark gray spheres). The light shaded polyhedra visualize the identity of the tetrahedral layers in $RE_3B_5O_{12}$ (RE = Er−Lu) (Figure 2) and semenovite.

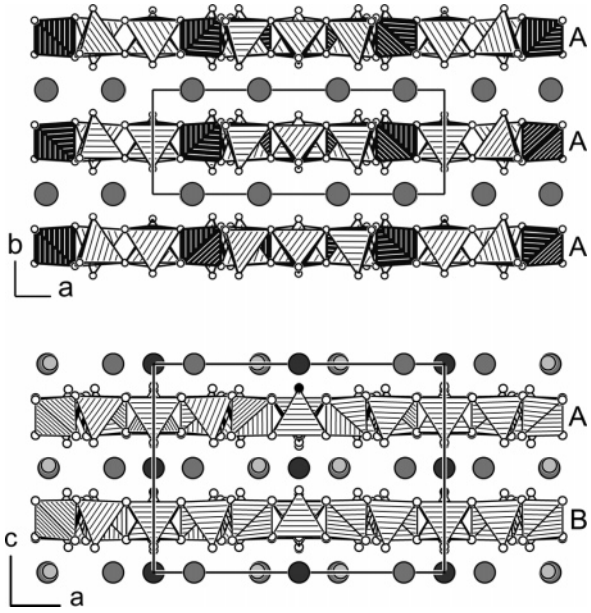

Figure 7. Comparison of the layer sequences in $RE_3B_5O_{12}$ (RE = Er−Lu) (top) and semenovite (space group: *Pmnn*) (bottom).

condensed layers of SiO_4- and BeO_4-tetrahedra. Figure 6 visualizes the structural relationship of $RE_3B_5O_{12}$ (RE = Er−Lu) compared with semenovite. The condensation of the tetrahedra is identical to the order in $RE_3B_5O_{12}$ (RE = Er−Lu). For a better understanding, the light shaded polyhedra in this figure of semenovite represent the same part of tetrahedra as shown in Figure 2. The structural peculiarities of semenovite (twin refinement) and the uncertainties in the chemical composition of the crystal, examined by X-rays, forced the authors to assume an idealized crystal structure in which the metal position M(1) was completely filled by RE and the site M(2) either remained empty or was occupied by variable amounts of sodium.[28,29] M(3) was completely filled by (Fe, Mn), M(4) was empty, and M(5) and M(6) were completely filled by (Ca, Na) and sodium, respectively. Another source of difficulties was the possible mutual substitution of silicon for beryllium according to the variations of the silicon content, indicated by the chemical analyses. Here the authors supposed that the tetrahedral sites T(1), T(2), T(4), T(6), and T(7) were centered by silicon, T(2) and T(4) by Si/Be (80%/20%), and T(3) and T(5) by Si/Be (20%/80%). Therefore, two geometrically similar layers are superposed in the unit cell at distance *c*/2, in which the main difference is given by the nature of the atoms at the center of two superposed tetrahedra. The compounds $RE_3B_5O_{12}$ (RE = Er−Lu) strictly possess boron in the center of the tetrahedra, upon which the unit cell axis *b* shows half the value of the corresponding *c*-axis in semenovite (Figure 7). Correspondingly, semenovite crystallizes in the space group *Pmnn* (standard setting: *Pnnm*, No. 58), which represents a maximal *klassengleiche* subgroup of index 2 (*a*, 2*b*, *c*) of the space group *Pmna* (No. 53). The enlarged unit cell in semenovite is required for ordering the metal atoms and the tetrahedral center with Si/Be. The first rare-earth site RE(1) in $RE_3B_5O_{12}$ (RE = Er−Lu) lies between the centers of the five-membered rings. This position corresponds to the sites M(5) and M(6) in semenovite, occupied by (Ca, Na) and sodium, respectively. The cavities between the eight-membered rings in $RE_3B_5O_{12}$ (RE = Er−Lu) are completely filled with rare-earth cations RE(2). In semenovite, these positions are separated in two M(1) sites or two M(2) sites, and M(1) is filled by RE and M(2) occupied by variable sodium amounts. Between the centers of the four-membered rings, the compounds $RE_3B_5O_{12}$ (RE = Er−Lu) exhibit no atoms, while in semenovite these M(3) and M(4) positions exhibit the octahedrally coordinated atoms Fe, Mn, Zn, Ti, and emptiness, respectively. Owing to the latter site, which is unoccupied in the rare-earth borates $RE_3B_5O_{12}$ (RE = Er−Lu), a consequential group−subgroup relationship between semenovite and the new compounds presented here is inadmissible. Nevertheless, the structures of $RE_3B_5O_{12}$ (RE = Er−Lu) represent homeotypes of the mineral semenovite. There exist related crystal structures such as amminofite $Ca_{12}(Si_{12}Be_8)(O, OH)_{48}$, which has a marked resemblance to semenovite. The total number of cations is the same, and the tetrahedral layer has an equal number of atoms, but the crystal structure is different (four- and six-membered rings). Hellandite is also to some extent comparable with $RE_3B_5O_{12}$ (RE = Er−Lu)/semenovite, in which the beryllium atoms are replaced by boron.[59] Hellandite represents a chain silicate. The filling of a vacant tetrahedral site would lead to a sheet silicate, of which the tetrahedral layers have the same kind and number of rings, though linked in a different way.

To examine the ring sizes in the here presented structures topologically, we calculated the cycle class sequences for $RE_3B_5O_{12}$ (RE = Er−Lu) and semenovite ((Fe^{2+}, Mn, Zn, Ti)RE_2Na_{0-2}(Ca, Na)$_8$(Si, Be)$_{20}$(O, OH, F)$_{48}$), specifying the relative abundance of B_nO_n/(Si, Be)$_n$(O, OH, F)$_n$ ring sizes (for n = 3−11) per unit cell.[60−63] The results are given in

(59) Mellini, M.; Merlino, S. *Am. Mineral.* **1977**, *62*, 89−99.

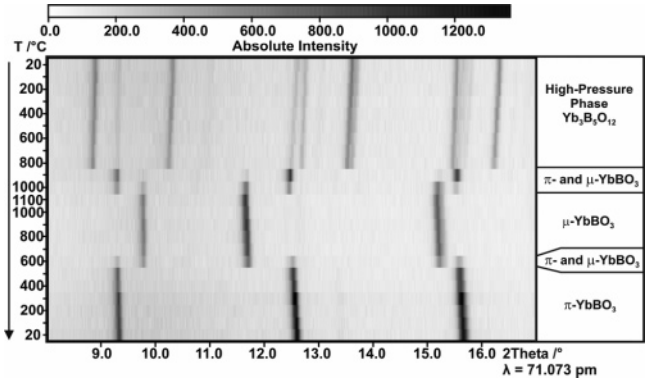

Figure 8. Temperature-dependent X-ray powder patterns, following the decomposition reaction of $Yb_3B_5O_{12}$.

Table 8. Obviously, the abundance of $(Si, Be)_n(O, OH, F)_n$ ring sizes in the unit cell of semenovite is not doubled in comparison to the abundance of B_nO_n ring sizes in the unit cell of $RE_3B_5O_{12}$ (RE = Er−Lu), as we would expect from the doubling of the *c*-axis in the structure of semenovite according to the *b*-axis in the structure of $RE_3B_5O_{12}$ (RE = Er−Lu). However, there is a small shift in the atom positions inside the different layers of semenovite along the *b*-axis, resulting in a different number of rings inside the unit cell of semenovite in relation to $RE_3B_5O_{12}$ (RE = Er−Lu). This leads to a calculated decrease in the relative abundance of $(Si, Be)_n(O, OH, F)_n$ ring sizes in the unit cell of semenovite.

Composition. The quantitative analysis on a sample of $Yb_3B_5O_{12}$ using ICP approved the composition of the new rare-earth borate affiliated from the crystal structure solution (theoretical: 67.8% Yb, 7.1% B; experimental: 67.1% Yb, 6.6% B; standard deviation: ±0.3%). These results were additionally verified using EDX (theoretical [atom %]: 15% Yb, 25% B, 60% O; experimental: 15% Yb, 25% B, 60% O).

Thermal Behavior of $Yb_3B_5O_{12}$. Different thermoanalytical investigations were performed to study the high-temperature stability and the metastable character of $Yb_3B_5O_{12}$.

Temperature-dependent X-ray powder diffraction on $Yb_3B_5O_{12}$ indicated several phase transitions (Figure 8). Successive heating of $Yb_3B_5O_{12}$ in the range of 800−900 °C led to a decomposition into a mixture of μ-$YbBO_3$ and π-$YbBO_3$. Further heating led to a complete transformation into the high-temperature polymorph μ-$YbBO_3$ in the range of 1000−1100 °C. Subsequent cooling showed a reappearance of the low-temperature polymorph π-$YbBO_3$ between 700 and 600 °C, and a complete transformation into π-$YbBO_3$ below 500 °C. These results are in agreement with the thermoanalytical measurements performed between room temperature and 1200 °C for $Yb_3B_5O_{12}$ (Figure 9). During heating, broad endothermic effects occur in the DTA between 844−933 °C and 934−1016 °C, owing to a decomposition of the compound into a mixture of μ-$YbBO_3$ and π-$YbBO_3$ and a following complete transformation of π-$YbBO_3$ into the high-temperature polymorph μ-$YbBO_3$. Any weight loss could not be observed in thermogravimetrical measurement between room temperature and 1200 °C. Therefore, we presume that the excess of B_2O_3, formed by the decomposition, was present as a glass.

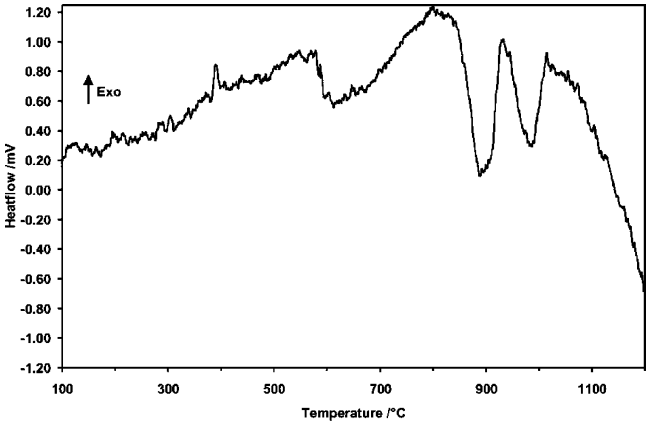

Figure 9. Difference thermal analysis curve of $Yb_3B_5O_{12}$ on heating.

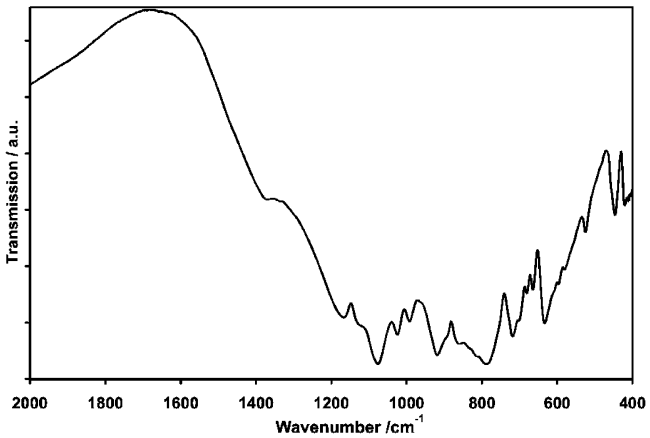

Figure 10. IR spectrum of $Yb_3B_5O_{12}$.

Vibrational Spectroscopic Characterization. Figure 10 shows the section 400−2000 cm^{-1} of the infrared spectrum of $Yb_3B_5O_{12}$. The absorption peaks between 790 and 1150 cm^{-1} are those typical for the tetrahedral borate group BO_4 as in YBO_3, $GdBO_3$, or $TaBO_4$.[64−66] Between 1250 and 1420 cm^{-1}, and below 810 cm^{-1}, we observe weak absorptions typical for triangular BO_3-groups as in $LaBO_3$,[67,68] and $Eu_2B_4O_9$.[69] As mentioned in the Introduction, the phases $RE_3B_5O_{12}$ were discovered during the syntheses of the meta-borates β-$RE(BO_2)_3$ (RE = Tm−Lu) as byproducts. An optimization of the syntheses led to nearly phase-pure compounds $RE_3B_5O_{12}$ (RE = Er−Lu); the byproducts were identified as the meta-borates β-$RE(BO_2)_3$. Since BO_3-groups are missing in $Yb_3B_5O_{12}$, the absorptions could be assigned

(60) Klee, W. E. *Z. Kristallogr.* **1987**, *179*, 67−76.
(61) Beukemann, A.; Klee, W. E. *Z. Kristallogr.* **1994**, *209*, 709−713.
(62) Beukemann, A.; Klee, W. E. *Z. Kristallogr.* **1992**, *201*, 37−51.
(63) Thimm, G.; Schumacher, S.; Uhr, W.; Klee, W. E. *TOPOLAN−Topological Analysis of Crystal Structures*; University of Karlsruhe: Karlsruhe, Germany, 1993.
(64) Ren, M.; Lin, J. H.; Dong, Y.; Yang, L. Q.; Su, M. Z.; You, L. P. *Chem. Mater.* **1999**, *11*, 1576−1580.
(65) Laperches, J. P.; Tarte, P. *Spectrochim. Acta* **1966**, *22*, 1201−1210.
(66) Blasse, G.; van den Heuvel, G. P. M. *Phys. Status Solidi A* **1973**, *19*, 111−117.
(67) Steele, W. C.; Decius, J. C. *J. Chem. Phys.* **1956**, *25*, 1184−1188.
(68) Böhlhoff, R.; Bambauer, H. U.; Hoffmann, W. *Z. Kristallogr.* **1971**, *133*, 386−395.
(69) Machida, K.; Hata, H.; Okuno, K.; Adachi, G.-Y.; Shiokawa, J. *J. Inorg. Nucl. Chem.* **1979**, *41*, 1425−1430.

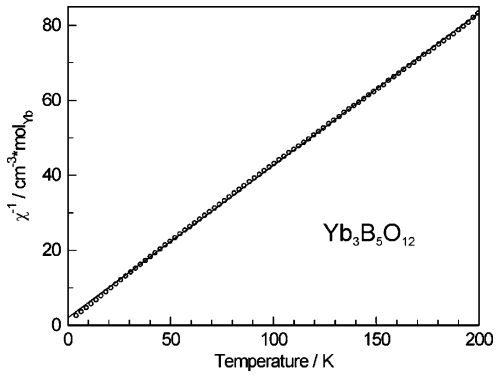

Figure 11. The reciprocal magnetic susceptibility of $Yb_3B_5O_{12}$, plotted as a function of temperature in the range 3−200 K. The measured data points are marked with circles, and the linear least-squares fitted Curie−Weiss function is indicated with a line. For details see text.

to the corresponding OB_3-vibrations of the small byproduct β-$Yb(BO_2)_3$.[31] Analogous geometrics and similar force parameters in the OB_3-group recommend this assignment because it is also valid for β-ZnB_4O_7,[70] β-CaB_4O_7,[71] $Na_3[B_6O_9(VO_4)]$,[72] and γ-$RE(BO_2)_3$ (RE = La−Nd).[33,34] The existence of four crystallographically independent BO_4-units in the structure of $Yb_3B_5O_{12}$ renders a detailed assignment of the broad bands more difficult. In the upper range (4000−2000 cm^{-1}) no absorption bands due to hydrogen (OH) could be found.

Magnetic Properties. The reciprocal susceptibility of $Yb_3B_5O_{12}$ as a function of temperature is plotted in Figure 11. As can be seen from that figure, $Yb_3B_5O_{12}$ exhibits Curie−Weiss behavior with a small negative Weiss constant ($\theta = -4.8(5)$ K), close to ideal free-ion paramagnetism. The calculated magnetic moment of 4.44(1) μ_B per Yb atom agrees well with the free-ion value of Yb^{3+} ($4f^{13}$ configuration, $^2F_{7/2}$) found in the literature ($\mu_{eff} = 4.54\ \mu_B$) according to $\mu_{eff} = g[J(J+1)]^{1/2}$.[73] No magnetic ordering was found within the measured temperature range. The slightly negative Weiss constant may be indicative of antiferromagnetic ordering at very low temperature.

Conclusions

In this paper, we described the multianvil synthesis of anhydrous rare-earth borates with the composition $RE_3B_5O_{12}$ (RE = Er−Lu) under extreme high-pressure/high-temperature conditions. This way it was possible to realize a new composition in the system RE_2O_3/B_2O_3 next to the formerly published compounds $RE_4B_6O_{15}$ (RE = Dy, Ho), α-$RE_2B_4O_9$ (RE = Eu−Dy), and β-$RE_2B_4O_9$ (RE = Dy, Gd)[74,75] by means of high pressure. According to the pressure coordination rule, all boron atoms exhibit exclusively tetrahedral oxygen coordination in the structures of $RE_3B_5O_{12}$ (RE = Er−Lu). The BO_4-tetrahedra are connected to layers that are separated and charge-balanced by the rare-earth cations. Repeatedly, we observed only the presence of BO_4-tetrahedra in borates synthesized under these high pressures. This favors the assumption that synthetic conditions of 10 GPa or higher lead primarily to tetrahedral boron coordination in borates. Lower pressures show the presence of BO_3-groups next to BO_4-tetrahedra, whereby the BO_3-part decreases with increasing pressure. With the given structural similarity between $RE_3B_5O_{12}$ (RE = Er−Lu) and the beryllo-silicate semenovite, we were able to realize a silicate-analogous structure, in which all tetrahedral positions, formerly occupied by Si/Be (semenovite), were completely substituted by boron for the first time (homeotype structure to semenovite). This confirms impressively that high-pressure enables the stabilization of boron on tetrahedral silicon positions in silicates. Furthermore, these results give direct evidence for the role of minerals in the upper crust, confirming that they may represent effective sinks for boron under the extreme conditions of high pressures and temperatures. As investigations concerning the structural chemistry of borates in the pressure range ≥10 GPa are rare, our examinations entered a new field of research with fundamental consequences for geological questions referring to the role of the element boron. Furthermore, the question of a higher coordination number (>4) at the element boron analogous to the element silicon should be commented on in this context: generally, it should be possible to increase the coordination number to five or probably six by use of high pressure, but we assume that nowadays the necessary pressure lies far beyond the technical possibilities. In this context, we observed that high pressure in the chemistry of borates can lead to edge-sharing BO_4-tetrahedra.[35−39] This structural motif was discussed in silicate chemistry on the example of "fibrous SiO_2" only once, without clear evidence of its factual existence.[76] In conclusion, the preparative access into the structural chemistry of borates under high pressure, using the multianvil technique, leads to interesting new insights, giving rise to detailed investigations in the pressure range ≥10 GPa.

Acknowledgment. We thank Dr. P. Mayer, Dr. H. Piotrowski (both Department Chemie and Biochemie, LMU München) and Dr. R.-D. Hoffmann (Universität Münster) for collecting the single-crystal X-ray data, Dipl. Chem. S. Correll (LMU München) for the in situ powder diffraction measurements, Dipl. Min. Sabine Schmid (LMU München) for DTA, H. Hartl for ICP, and Prof. Dr. W. Schnick (LMU München) for the continuous support of these investigations. This work was financially supported by the Deutsche Forschungsgemeinschaft and the European Science Foundation within the COST D30 network (D30/003/03). M. Valldor is indebted to the Alexander-von-Humboldt Foundation for a research stipend.

Supporting Information Available: Crystallographic information (CIF). This material is available free of charge via the Internet at http://pubs.acs.org.

CM047741+

(70) Huppertz, H.; Heymann, G. *Solid State Sci.* **2003**, *5*, 281−289.
(71) Huppertz, H. *Z. Naturforsch., B: Chem. Sci.* **2003**, *58*, 257−265.
(72) Touboul, M.; Penin, N.; Nowogrocki, G. *J. Solid State Chem.* **2000**, *150*, 342−346.
(73) Lueken, H. *Magnetochemie*; Teubner: Stuttgart, Germany, 1999.
(74) Huppertz, H.; Altmannshofer, S.; Heymann, G. *J. Solid State Chem.* **2003**, *170*, 320−329.
(75) Emme, H.; Huppertz, H. *Acta Crystallogr., Sect. C: Struct. Commun.* **2005**, 61, i23−i24.
(76) Weiss, A.; Weiss, A. *Z. Anorg. Allg. Chem.* **1954**, *276*, 95−112.
(77) Herrendorf, W.; Bärnighausen, H. *HABITUS−Program for Numerical Absorption Correction*; University of Karlsruhe/Giessen, Germany, 1993/1997.